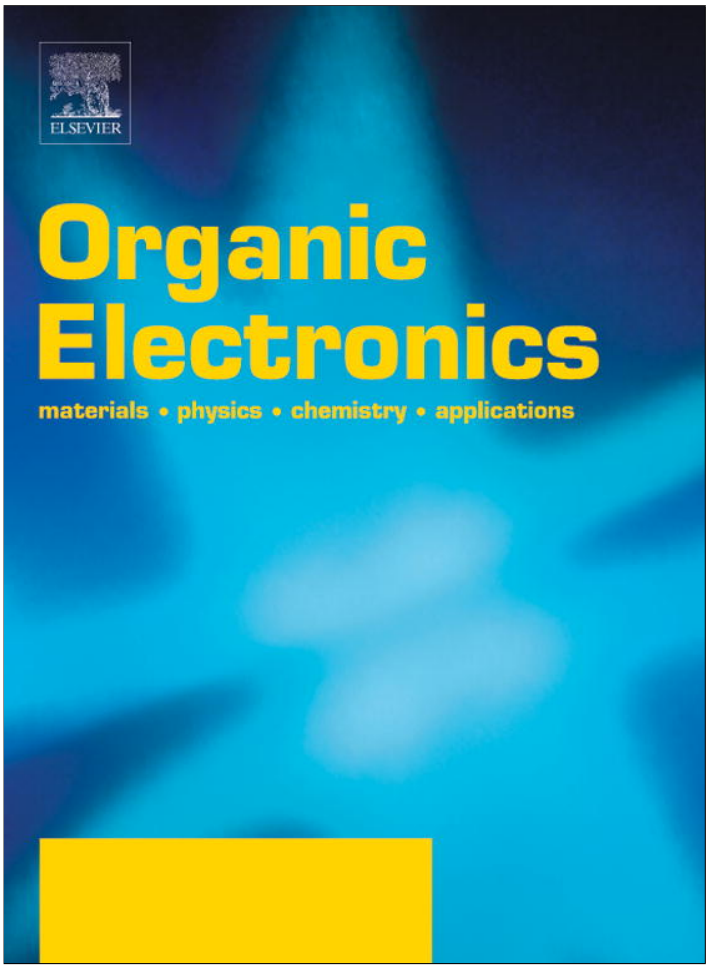

(This is a sample cover image for this issue. The actual cover is not yet available at this time.)

Organic Electronics 13 (2012) 1844–1852

Contents lists available at SciVerse ScienceDirect

Organic Electronics

journal homepage: www.elsevier.com/locate/orgel

Melanin films on Au(1 1 1): Adsorption and molecular conductance

Alejandro González Orive [a], Alberto Hernández Creus [a], Pilar Carro [a,b,*], Roberto C. Salvarezza [b]

[a] Departamento de Química Física, Instituto Universitario de Materiales y Nanotecnología, Universidad de la Laguna, La Laguna, Tenerife, Spain
[b] Instituto de Investigaciones Fisicoquímicas, Teóricas y Aplicadas (INIFTA), CONICET-Universidad Nacional de La Plata, Sucursal 4, Casilla de Correo 16, La Plata 1900, Argentina

ARTICLE INFO

Article history:
Received 16 February 2012
Accepted 18 May 2012
Available online 7 June 2012

Keywords:
Melanin films
Gold
Electronic properties
STM
Photoconductivity

ABSTRACT

We have studied the adsorption and electronic properties of thin melanin films on Au(1 1 1) by scanning tunneling microscopy (STM), scanning tunneling spectroscopy (STS), and density functional (DF) calculations. We have found that the minimum melanin unit detected under different adsorption conditions is consistent with the structural model for eumelanin protomolecules based on tetramer macrocycles formed by four monomer units (hydroquinone, indolequinone and its tautomers) with an inner porphyrin ring. DF calculations reveal that the entire π structure of the tetramers is implied in the chemisorption process through its frontier orbitals (HOMO and LUMO), a fact that is reflected in the change of intramolecular bonds. Also van der Waals interactions give an important contribution to the adsorption energy (≈0.02 eV/Å^2). Dried thin melanin films (1 monolayer in thickness) exhibit good electronic conductance due to the presence of localized states near the Fermi level while dried thicker films exhibit a semiconductor-like behavior. Illumination of the thicker films with white light results in significant photo-induced tunneling currents when the melanin-covered Au is made negative with respect to the tip.

1. Introduction

Melanins are one class of biopolymers with interesting physical and chemical properties such as photoactivity, electrochemical response, and amorphous semiconductor behavior [1,2]. The combination of optical and electronic properties in melanins has drawn the attention of scientists as potential materials for organic solar cells and other novel electronic devices. In fact, melanins exhibit a broad band absorption which may be suitable for their use as sensitizers in photovoltaic devices [3]. In particular, synthetic eumelanin, formed by 5,6-dihydroxyindole (DHI) (Fig. 1a) and 5,6-dihydroxyindole-2-carboxylic acid (DHICA) monomers (Fig. 1b) is chemically and photochemically very stable.

Recent *ab initio* calculations have shown that the Highest Occupied Molecular Orbital (HOMO)–Lowest Occupied Molecular Orbital (LUMO) gaps of the DHI redox forms are appreciably different [4]. In addition, it has been recently demonstrated that several redox forms of DHI and DHICA are thermodynamically stable [5,6]. Hence, it can be concluded that a wide variety of "chemically distinct" oligomers, each with a different HOMO–LUMO gap, could be formed. However, it is still under debate how the DHI and DHICA monomers organize into 4 or 5 oligomer nano-aggregates. A clear idea of the basic structural units is fundamental to develop a consistent model for condensed phase charge transport in such complex bioorganic materials. In fact, while melanins in the condensed phase have been described as amorphous semiconductors [7,8] there is still no agreement if the observed conductivity is electronic in nature [3]. Thus, the production of thin melanin films with defined structure on conducting substrates is a crucial point for study the electric conductance of this type of biopolymers.

* Corresponding author at: Departamento de Química Física, Instituto Universitario de Materiales y Nanotecnología, Universidad de la Laguna, La Laguna, Tenerife, Spain. Tel.: +34 922 318031; fax: +34 922 318002.
E-mail address: pcarro@ull.es (P. Carro).

1566-1199/$ - see front matter © 2012 Elsevier B.V. All rights reserved.
http://dx.doi.org/10.1016/j.orgel.2012.05.033

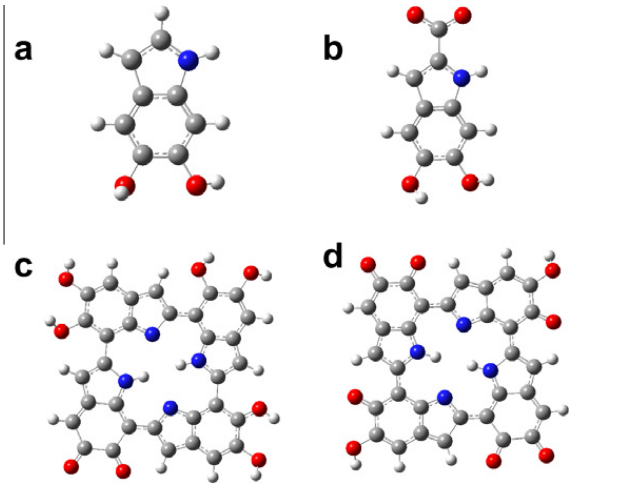

Fig. 1. (a) DHI, (b) DHICA, (c) IHHH tetramer, (d) IMIM tetramer. N: blue, C: grey, O: red; H white. (For interpretation of the references to colour in this figure legend, the reader is referred to the web version of this article.)

Recently we have shown that ultrathin films of eumelanins can be electrochemically deposited on Au(1 1 1) [9] and highly oriented pyrolityc graphite [10] from alkaline solutions containing synthetic eumelanin. In this case, the film exhibits the hierarchical structure found in natural melanin with melanin aggregates with sizes ranging from ≈2 to 50 nm [9,11]. The melanin films on Au(1 1 1) are interesting as a model system to study the initial adsorption stage of melanin on well ordered surfaces, their conductance and photoelectric properties.

Scanning tunneling microscopy (STM) and scanning tunneling spectroscopy (STS) are powerful methods for imaging and probing locally the electronic properties of melanin films under light irradiation. In this work we report a combined experimental/theoretical study of dried ultrathin synthetic eumelanin films electrochemically deposited on Au(1 1 1) substrates from aqueous 0.1 M NaOH melanin-containing solutions by means STM and STS measurements. We have also used density functional theory (DFT) to obtain the structural information, the adsorption energy and electronic structure of the melanin protomolecule adsorbed on Au(1 1 1). The chemical models used in this work are two tetramer macrocycles proposed in the literature as building blocks of the biopolymer since they reproduce accurately several important properties of eumelanin as X-ray scattering data, its ability to capture and release ions, the experimental features of its spectrum and the characteristic size of the protomolecules [12,13]. One tetramer (IHHH) consists in three hydroquinones and one indolequinone units (Fig. 1c) and the other (IMIM) consists in two indolequinone and two tautomers quinone-methide units (Fig. 1d).

Results from these calculations show that adsorbed IMIM tetramer exhibits structural and electronic data consistent with those experimentally measured on dried thin melanin films deposited on Au(1 1 1). These films have a good electronic conductance that can be explained by the presence of localized states near the Fermi level. Experimental data shows that increasing the thickness of the dried films changes the electronic response to that exhibit by semiconductor-like organic films with an asymmetric photo-induced tunneling current response according to the bias voltage applied between the sample and the tip.

2. Experimental

2.1. Melanin preparation

Melanin deposits were electrochemically prepared as described in Ref. [9–11]. Briefly, the Au(1 1 1) substrates were immersed in a synthetic eumelanin-containing aqueous 0.1 M NaOH solution (0.3 g L^{-1}, melanin from Sigma, M8631). The Au(1 1 1) substrate was polarized at -1.0 V in a conventional three-electrode (working, reference and counter electrodes) electrochemical cell containing the melanin solution for different times (t = 10 min, 45 min, 120 min) in order to form the melanin film. Occasionally, melanin was adsorbed on the Au substrate under open circuit conditions (OCP) from the same melanin containing solutions for t = 10 min. The films were rinsed with water and carefully dried under nitrogen flux. It has been reported that the electrical properties of melanin changes from electro to proton conduction for humidity levels greater than 40% [3]. Therefore all our measurements were made al humidity levels well below this value.

2.2. Structural and electronic characterization

Structural data and electronic properties of the melanin films on Au(1 1 1) were determined by scanning tunneling microscopy (STM) and scanning tunneling spectroscopy (STS) measurements using a scanning tunneling microscope (Nanoscope IIIa, Veeco Instruments) operating in air at room temperature. Pt–Ir tips were used for these measurements. I (tunneling current) vs V (bias voltage) curves were averaged over at least three different regions of the samples. In STS measurements positive bias means that the sample is made positive. The dI/dV plots shown in this paper are the average of ten measurements. These measurements were taken under the same experimental conditions and performed on different regions of the samples.

2.3. Photocurrent measurements

The experimental setup consisted of a simple photographic white light flash focused on the tip-sample gap during only 1 ms. The flash was set 40 cm far away from the tip at an incident angle of 15°. In these conditions a power density of 3 mW cm^{-2} could be measured at the sample surface. The tip was approached under no illumination till to obtain tunneling effect under different conditions. In particular experiments were made using four bias potential, ±500 mV and ±200 mV, combined with two tunneling current, 300 pA and 600 pA. In every case, once the tunneling current was set, the operation mode was changed from the constant current mode (the standard topographic STM mode) to the constant height mode, i.e. the Z piezotube feedback loop is disconnected. In this way and without scanning the tip to keep constant the

tip-sample distance, the sample was irradiated during a 1 ms long light pulse. Immediately, an important enhancement in the flowing tunneling current was registered. It should be noted that in order to warrant the constancy in the tip-sample separation, changes in the bias potential sign were always made without withdrawing the tip.

2.4. Computational details

The calculation was performed using plane-wave pseudopotential periodic DFT. The exchange–correlation potential was described by means of the generalized gradient approach (GGA) with the Perdew–Wang (PW91) [14] implementation. The one-electron wave functions have been expanded on a plane wave basis set with a cut-off of 450 eV for the kinetic energy. The Brillouin zone sampling was carried out according to the Monkhorst–Pack [15] scheme with $(3 \times 3 \times 1)$ dense k-points meshes. The projector augmented wave (PAW) method [16,17], as implemented by Kresse and Joubert [18], has been employed to describe the effect of the inner cores of the atoms on the valence electrons. The energy minimization (electronic density relaxation) for a given nuclear configuration was carried out using a Davidson block iteration scheme. The dipole correction was applied to minimize polarization effects caused by asymmetry of the slabs. All calculations have been carried out using the VASP 5.2.11 package [18,19].

As it is well known, the long-range van der Waals forces are undoubtedly important in the interaction between organic molecules and metal surfaces. Then, van der Waals (vdW) intermolecular forces will play a relevant role in the system studied in this work. Moreover one of the main shortcomings of GGAs functionals is the inability to describe non-local vdW dispersion forces. In order to account for the vdW interactions we have employed the semiempirical DFT-D [20] method of Grimme [21] as implemented in the VASP 5.2.11 package. This vdW dispersion correction has the form C_6R^{-6} and the value for Au atom has been taken from the value given by Grimme, very similar to the value derived by a hybrid quantum mechanics (QM) approach in the literature [22]. We have also done calculations without the vdW correction in order to evaluate the influence of this kind of interaction.

The surface was modeled by a periodic slab composed of four metal layers and a vacuum of ~12 Å. Adsorption occurs only on one side of the slab. During the geometry optimization the two bottom layers were kept fixed at their optimized bulk truncated geometry for the Au(1 1 1) surface. The two outermost atomic metal layers, as well as the atomic coordinates of the adsorbed species, were allowed to relax without further constraints. The atomic positions were relaxed until the force on the unconstrained atoms was less than 0.03 eV/Å. The unit cell employed in the calculation was a $(5 \times 3\sqrt{3})$ of the Au(1 1 1). The calculation of the isolated tetramers has been done in a supercell with side lengths of (20 Å × 20 Å × 10 Å). The lattice parameter calculated for bulk Au was 4.18 Å.

The adsorption energy (E_{ads}) of the corresponding tetramer have been defined by

$$E_{ads} = [E^{tetramer/Au} - E^{Au} - E^{tetramer}] \quad (1)$$

where $E^{tetramer/Au}$, E^{Au} and $E^{tetramer}$, stand for the total energy of the system, the energy of the clean surface, and the energy of the IHHH/IMIM tetramer, respectively. Negative numbers indicate an exothermic adsorption process with respect to the clean surface and the isolated tetramer originated during the adsorption process.

3. Results

3.1. STM imaging

First we study the initial stage of adsorption to detect the smallest melanin units present on the Au(1 1 1) surface. This was experimentally done by adsorbing melanin at OCP for t_a = 10 min on the Au(1 1 1) surface. In fact, STM imaging of the Au(1 1 1) surface after immersion in the melanin containing solution reveals small units 1.6–3.2 nm in average size and ≈0.3 nm in average height (Fig. 2a), a figure similar to the layer–layer separation found in graphite. The presence of these structural elements on the Au(1 1 1) surface are clearly seen in the power spectral density (PSD) analysis of the images that exhibits peaks in the 1.6 to 3.2 nm range (Fig. 2b). These results are consistent with the presence of a melanin protomolecule and small oligomers with a graphite-like structure. The smallest 1.6 nm units have a size very close to that expected for the melanin tetramers shown in Fig. 1c and d (1.5 nm in size) while the 3.2 nm structures could correspond to small oligomers formed by four tetramers as shown in Fig. 2c. However, the film grown under OCP conditions is discontinuous exposing bare Au areas as revealed by STM images taken at different places of the sample (data not shown). In order to improve the film quality we have prepared the melanin films by adsorbing melanin from the solution with the Au(1 1 1) surface polarized at −1.0 V for t_a = 10 min. In this case the Au(1 1 1) surface is almost covered by the 3.2 nm oligomers as shown in Fig. 2d and e.

The increase in the deposition time (t_a = 45 min) results in the formation of more compact films consisting of larger aggregates. In fact, the STM images (Fig. 3a) and PSD analysis (Fig. 3b) reveal an average aggregate size of ≈17 nm. However, the influence of the Au(1 1 1) substrate is still visible since the typical triangular features of this face are clearly seen on the image. This fact indicates that the melanin film involves only a few monolayers. In fact, assuming that the ≈1 nm maximum aggregate height in Fig. 3c reflects the film thickness (h) and taking 0.33 nm interlayer separation we can estimate $h \approx 3$ monolayers.

The structure of the melanin oligomers shown in Fig. 2c explains the incorporation of metallic cations in the tetramer lattice, an important property of melanin films. In fact, each tetramer exhibits the oxygen atoms at its outer edge and the nitrogen atoms located in a porphyrin hole in its center. Therefore, there are two possible environments for cation coordination: one created by the 4 O atoms of 4 adjacent tetramers and the other 4 N atoms at the center of each porphyrin ring. Previous XPS data of Fe containing melanin films on Au(1 1 1) (t_a = 100 min) indicates that O is

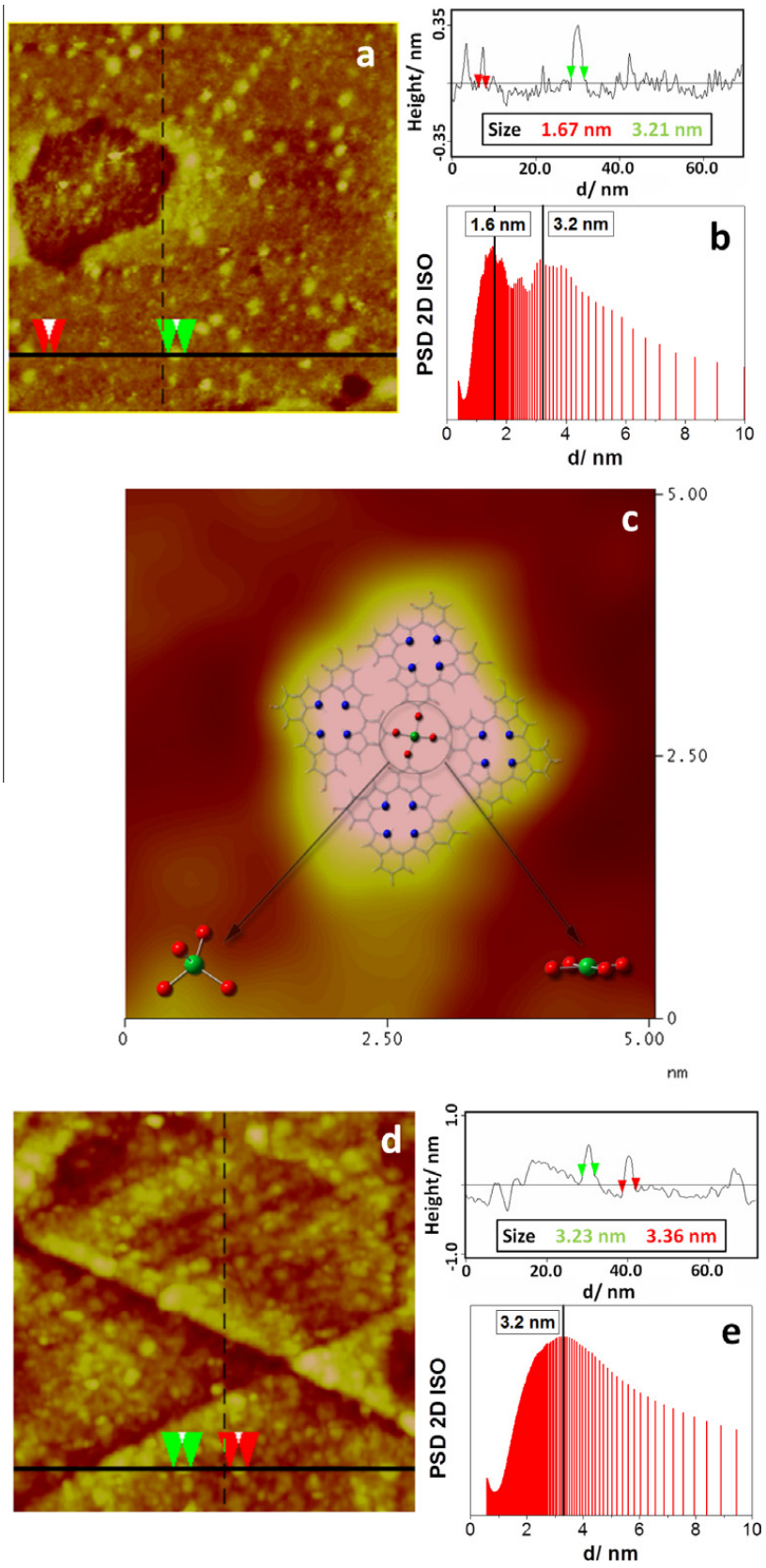

Fig. 2. 70×70 nm^2 STM images of the Au(1 1 1) surfaces after immersion in the melanin-containing 0.1 M NaOH solution (c = 0.3 g L^{-1}) for: (a) 10 min at OCP, (d) 10 min at $E = -1.0$ V. The black solid lines in panels (a) and (d) indicate the places where the cross-sections (right) were made. (b) and (d) Isotropic 2D power spectral densities performed on the images shown in (a) and (d), respectively. The black lines indicate the average particle size (c) 5×5 nm^2 STM image of a 3.2 nm size particle. A scheme of 4 tetramers forming an oligomer is superimposed on the STM image. The coordination site for a Fe ion is indicated. Bottom at the right side: tetrahedral site, bottom at the left side: octahedral site. Blue: N, red: O, green: Fe. All STM images were taken at a bias voltage = 1.0 V and tunneling current = 0.35 nA. (For interpretation of the references to colour in this figure legend, the reader is referred to the web version of this article.)

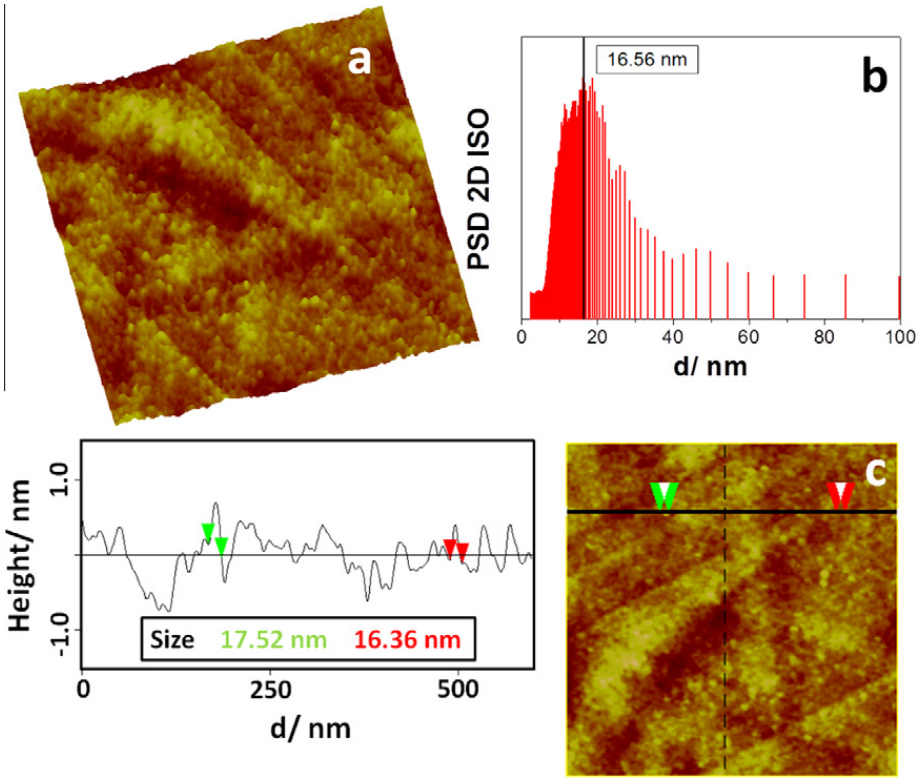

Fig. 3. (a) Three-dimensional ($600 \times 600\ nm^2$) image of the Au(1 1 1) surface after immersion in the eumelanin-containing 0.1 M NaOH solution ($c = 0.3\ g\ L^{-1}$) for 45 min at −1.0 V. $Z = 5$ nm. (b) Isotropic 2D power spectral density performed on the image shown in (a). The black line indicates the average particle size. (c) A representative cross-section of a $600 \times 600\ nm^2$ STM image showing individual 8–22 nm sized melanin particles on the Au(1 1 1) surface is shown. The black solid line in panel d indicates the place where the cross-section was made. STM images were taken at a bias voltage = 1.0 V and tunneling current = 0.35 nA.

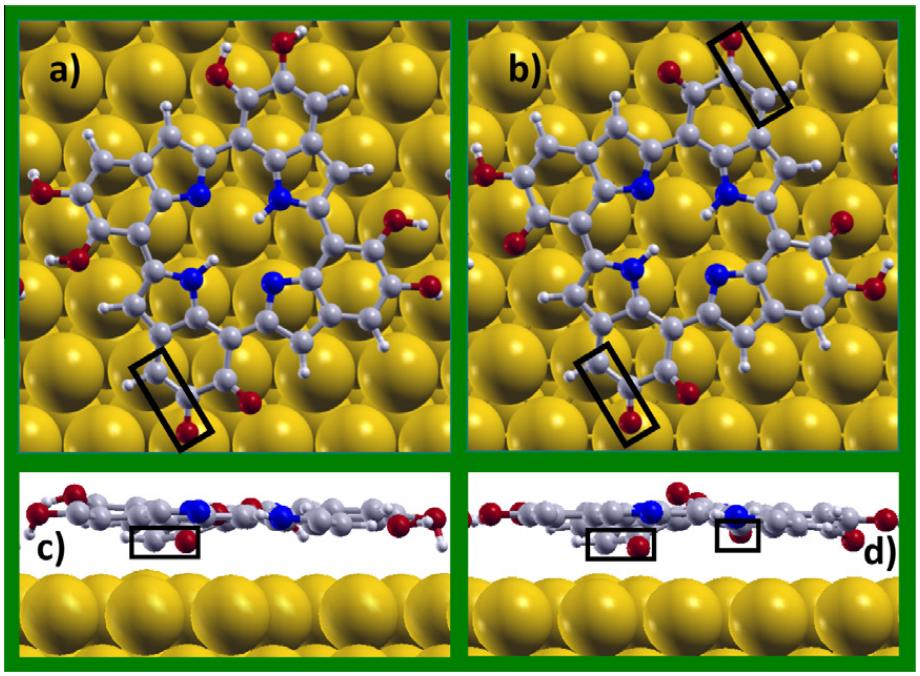

Fig. 4. Top view of the optimized geometry of the IHHH (a) and IMIM (b) tetramers on Au(1 1 1) surface. (c and d) Side view of the adsorbed systems. Blue: N: gray: C: red: O, white: H; golden: Au. (For interpretation of the references to colour in this figure legend, the reader is referred to the web version of this article.)

the preferred environment for Fe ions [23]. In fact, the N 1s spectra show two components located at binding energies (BE) of 399 eV and 400.3 eV. These BE values are not consistent with metallic cation-N atoms coordination in the

porphyrin rings that show a BE at 398.4 eV [24]. In a 1 monolayer thick melanin films the metallic cation should interact with the Au surface while for multilayered films the cation would lie between a pair of planar sheets contained in the melanin oligomers.

3.2. Modeling melanin adsorption on Au(1 1 1)

In the next we analyze the adsorption of the melanin units on the Au(1 1 1) by using DF calculations. Fig. 4a–d show the relaxed geometry of the IHHH and IMIM tetramers.

The adsorbates have been placed on top the Au(1 1 1) surface with the molecular plane parallel to the metal surface (Fig. 4a and b). This configuration was selected based on the STM images where the melanin oligomers have ≈0.3 nm in height (Fig. 2d) indicating that they are lying parallel to the substrate. This is not surprising since the oligomers are formed at −1.0 V, i.e. a potential more negative than the zero charge potential (zcp) of the Au(1 1 1) face [9]. In fact, it has been shown that the adsorption of nitrogen containing ring molecules such as pyridine takes place parallel to the Au(1 1 1) surface when the Au(1 1 1) is negatively charged but stands up at potentials more positive than the zero charge potential of the substrate [25]. It has also been reported that pyridine and pyrazine molecules at negative applied potentials involve π orbital interactions with the Au surface, whereas at positive applied potentials it is the N lone-pair the responsible of the interaction with the metal surface [26]. Therefore, the adsorption of the tetramers in a parallel configuration with respect to the Au(1 1 1) surface is justified.

The tetramer IHHH/IMIM relaxed geometry is slightly bended from the initially flat isolated molecules (Fig. 4c and d). The average height of the tetramer atoms above the topmost substrate layer is 0.3 nm in agreement with the STM images. We note that the carboxylic oxygen in C5 and the carbon C4 of indolequinone fragments (indicated by a black rectangle in Fig. 4) are closer to the Au surface atoms (O: 0.24 nm, C: 0.24 nm) than the rest of the atoms in both tetramers. These results agree with first-principle density functional theory calculations for tryptophan-Au nanoparticles where the binding was assigned to both carboxyl and indole groups [27]. Note that the tetramer loses certain degree of π conjugation upon adsorption as the intramolecular structure of the tetramers undergo some subtle changes, for instance the C = O bond in the C5 becomes longer upon adsorption.

The calculated adsorption energies (E_{ad}) of the tetramers without considering van der Waals (vdW) interactions are −1.25 eV for IMIM and −0.71 eV for IHHH. The magnitude of these values indicates a relatively weak chemisorption process. Note that simply physisorption can be discarded because the shortest distance between the Au surface atom and the C atom below is 0.24 nm, a distance smaller than the sum of vdW radii of Au (0.166 nm) and C (0.17 nm). However, when vdW interactions are included in the calculations the adsorption energies remarkably raise to −6.4 eV for IMIM and −5.7 eV for IHHH, i.e. ≈−1.5 eV for monomer unit. These results indicate that vdW forces are crucial to strongly bind the tetramers to the Au(1 1 1) surface. This is not surprising as similar results have been reported for the adsorption of other aromatic molecules on metal surfaces when the dispersion forces are included in the calculations [28–31].

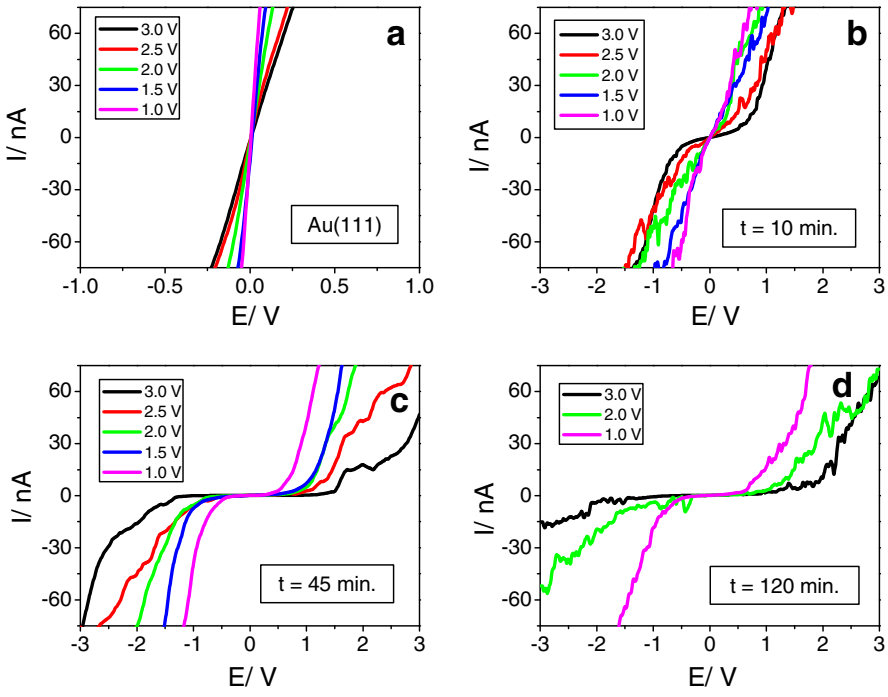

Fig. 5. *I* vs *V* curves recorded at different tip-sample distances determined by the set point bias voltage and current. The set-point bias voltages are indicated in the upper left panels (1–3 V), the set-point current was always 0.35 nA: (a) Au(1 1 1), (b) melanin film t_a = 10 min, (c) melanin film t_a = 45 min, and (d) melanin film t_a = 120 min.

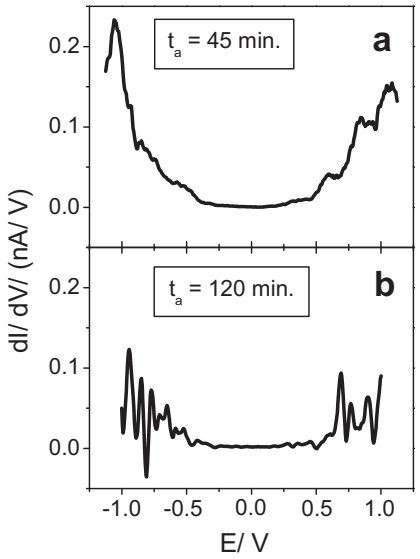

Fig. 6. *dI* vs *dV* curves measured for melanin films, (a) t_a = 45 min, and (b) t_a = 120 min. Sample bias: 1 V. The current used in all spectra was 0.35 nA.

We have performed a Bader analysis to evaluate the redistribution of the charge upon adsorption on Au(1 1 1) surface. The largest difference in this value is presented by the surface nearest carbon atoms (outlined in Fig. 5) which gain from the Au surface −0.12 e and −0.21 e for IHHH and IMIM tetramer, respectively. On the other hand, the O atom in the C=O group of the indolequinone fragment loses charge becoming +0.33 e more positive in both tetramers.

It is also interesting to note that the Au(1 1 1) work function changes only 0.1 eV after tetramer adsorption. This fact could be interpreted considering that the reduction of the intrinsic metal surface dipole is almost perfectly compensated by the surface dipole arising from Au to molecular-LUMO charge transfer.

3.3. Electronic characterization

The electronic properties of melanin films on Au(1 1 1) were experimentally studied using STS. Typical *I* vs *V* curves recorded for Au(1 1 1) and melanin films grown on Au(1 1 1) for different t_a under the same experimental conditions are shown in Fig. 5. Prior to record each STS curve the tip-sample distance was varied by changing the bias voltage between 1 and 3 V at a constant tunneling current of 0.35 nA. Note that a higher set-point bias voltage corresponds to a larger tip-sample distance if the set-point current is kept constant.

We first discussed the averaged *I* vs *V* plots for thin melanin- films (t_a = 10 min, ≈1 monolayer thick) on Au (Fig. 5b) comparing them with those recorder for Au(1 1 1) (Fig. 5a). It is evident that the *I* vs *V* curves for the thin melanin films approaches the behavior of the metallic conductor [32]. In contrast, the *I* vs *V* plots for thicker melanin films grown for t_a = 45 min (Fig. 5c) and for t_a = 120 min (Fig. 5d) on the Au(1 1 1) substrate exhibit a response characteristic of semiconductor materials [33]. In fact, a non-linear current region that slightly increases with the deposition time can be oberved. This is more clearly seen using the derivative tunneling spectra, *dI/dV* which is a measure of the local density of states (LDOS) of a surface [34].

The averaged derivative STS spectra shown in Fig. 6 for the thicker melanin films corresponds to the *I* vs *V* plots obtained at a sample-tip separation condition given by sample bias of 1.0 V and a tunneling current of 0.35 nA.

In these plots we note that for the film grown for t_a = 45 min the HOMO and LUMO are located at −0.5 and +0.6 eV, respectively while they move to −0.6 eV and +0.7 eV for t_a = 120 min. The magnitude of the gap is consistent with that already reported for semiconductor melanin films [1,35].

In the next we will analyze in more detail the behavior of the thin melanin film (t_a = 10 min, 1 monolayer thick) in order to explain its good electronic conductance. In particular we will compare the *dI* vs *dV* behavior of the thin melanin film with the projected density of states of IHHH and IMIM tetramers adsorbed on Au(1 1 1) surface from the DFT calculations.

The projected density of states (PDOS) onto the IHHH and IMIM tetramers are depicted in Fig. 7a and b, respectively. It can be seen that molecular energy levels of both tetramers hybridize with the delocalized metallic wave functions of the substrate showing a significantly amount of broadening originating a charge transfer between the

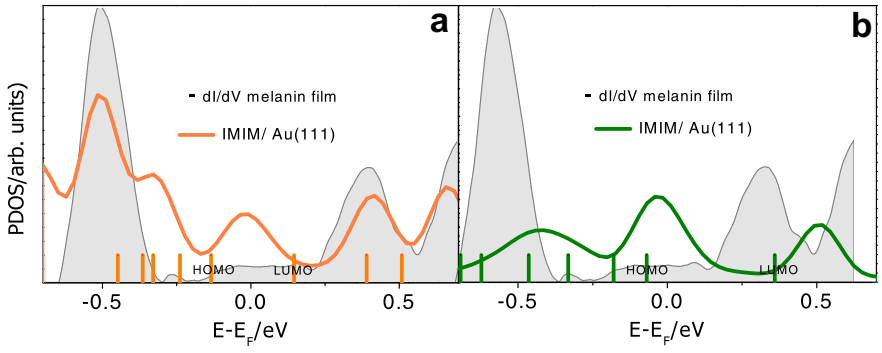

Fig. 7. The density of states projected (PDOS) onto (a) IMIM on Au(1 1 1) (orange line) and (b) IHHH on Au(1 1 1) (green line). The energy zero is taken to be the Fermi energy of the adsorbed system. Filled grey curve: *dI/dV* curve for thin melanin films (t_a = 10 min). The vertical bars indicate the electronic states for the isolated tetramers in vacuum. The HOMO and LUMO positions of the isolated tetramers in vacuum are indicated. (For interpretation of the references to colour in this figure legend, the reader is referred to the web version of this article.)

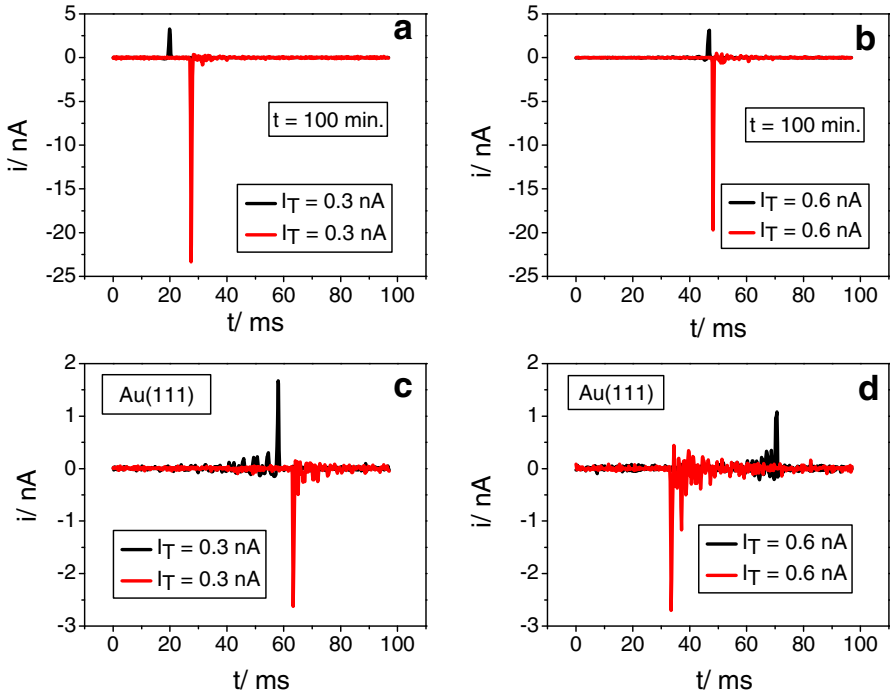

Fig. 8. Change in the tunneling current recorded in the constant height mode after a flash light pulse under different bias voltage (in the gap) and a constant tip-sample distance. (a and b) Melanin-covered Au(1 1 1), t_a = 100 min, tunneling current (a) I_T = 0.3 nA, (b) I_T = 0.6 nA. (c and d) Au(1 1 1), (c) I_T = 0.3 nA, (d) I_T = 0.6 nA. Bias voltage: E_B = +200 mV (black line) and E_B = −200 mV (red line). (For interpretation of the references to colour in this figure legend, the reader is referred to the web version of this article.)

tetramer and the substrate as revealed by the Bader charge analysis.

Although the GGA functionals fail to give an accurately prediction of HOMO and LUMO eigenvalues, they give a reasonable estimation of the HOMO–LUMO gaps [36]. However, in the thin melanin films adsorbed on Au(1 1 1) localized states appear filling the gap (see the experimental *dI/dV* plot in Fig. 7). Our DFT calculations also indicate the presence of electronic states in the Fermi level due to the strong hybridization of molecular orbitals and the substrate electronic states in the tetramer/Au interface. The state in the gap could correspond to the LUMO occupation of the tetramer. This orbital seems to shift towards lower energies lying now at the Fermi level. Note also that LUMO is partially filled in the adsorbed state reflecting the charge transfer from the Au surface. For both tetramers HOMO and LUMO orbitals lose their identity, the gap is practically disappeared, and, accordingly, the film exhibits metallic-like conduction.

At this point, we can return to the features related with the chemisorption mechanism of IMIM and IHHH tetramers on the Au(1 1 1) surface. As in the majority of large π-conjugated organic molecules with functional groups the bonding interactions can be understood through two cooperative mechanisms: (i) the Au surface transfers charge into the LUMO that it is placed at the Fermi level upon adsorption process and (ii) a local Au-O bonding between the carboxylic O to the Au(1 1 1) surface. It means that the entire π structure of the tetramer must be implied in the chemisorption process through its frontier orbitals (HOMO and LUMO) being reflected in the change of certain intramolecular bonds.

3.4. Photo-induced tunneling currents under white light illumination

We have used the STS setup to measure the photo-induced tunneling current between the tip and thick melanin film-covered Au(1 1 1) (t_a = 100 min, $h > 10$ monolayers) under illumination with a flash of white light. Our results for small bias lying in the gap (−200 mV, +200 mV), where no significant tunneling currents should be detected (see Fig. 5c and d) are shown in Fig. 8a and b. They show typical responses of tunneling currents as a function of the sign of the applied bias after a flash light pulse. These figures correspond to the results average over at least one hundred light pulses.

When the bias potential was set at positive values (sample positive) a small increment (ranging 1–3 nA) in the tunneling current is observed irrespective of the sample-tip distance (controlled by initial bias and tunneling current) (Fig. 8a and b). In contrast, when the bias potentials were negative (sample negative) a drastically increase in the tunneling current (ranging 15–25 nA) can be detected. The observed increments in tunneling currents for the negative bias voltage are much larger than those observed for clean Au(1 1 1) under the same experimental conditions (Fig. 8c and d). However, it is known that under illumination of photoactive materials in STS experiments an increase in the tunneling current is in general observed due to both the thermal expansion of the tip and the sample, which means a decrease in the tip-sample separation [37,38], and the possible contribution from photoinduced electrons related with the light pulse. The asymmetric increase in the measured tunneling current depending on

the bias voltage irrespective of the tip-sample distance (controlled by the tunneling current) allows us to discard the thermal expansion as the main contribution to tunneling current detected in our experiments. Therefore, as our STS results are taken in the gap region the photocurrents can be related to a photovoltaic effect in agreement with previous short circuit current measurements of thick melanin deposited on titania [3]. However, it is interesting to note that the asymmetric response with the bias observed in our experiments has not been reported yet for melanin films. Our results point up that while keeping constant the tip-sample distance and the absolute bias potential negative, an important flow of photo-induced electrons tunnels from the sample to the tip while the flux in hindered for positive bias. We propose that under illumination electrons move from the melanin film's HOMO to the LUMO where they are collected by the positively charged tip. Finally it should be noted that the production of a photocurrent under white light illumination is indicative of a semiconductor-like behavior which are in well agreement with the behavior of the *I* vs *V* plots recorded for the thicker melanin films.

4. Conclusions

The adsorption and electronic properties of thin melanin films on Au(1 1 1) is studied by using STM, STS and DF calculations. STM data demonstrated that smallest melanin units in the early stages of adsorption have similar sizes than IMIM and IHHH tetramers and small oligomers formed by these tetramers. DF calculations reveal that the entire π structure of the tetramers is implied in the chemisorption process through its frontier orbitals (HOMO and LUMO) being reflected in the change of certain intramolecular bonds. Dried thin melanin films exhibit a good molecular conductance due to the presence of localized states at the Fermi level. Thicker films exhibit semiconductor behavior with HOMO–LUMO separation of $\approx$1 eV. These films exhibit photo-induced tunneling current when illuminated with a flash of white light, its magnitude depending on the sing of applied bias.

Acknowledgments

This paper was financially supported by projects from MICINN (Spain, CTQ2008-06017/BQU, CTQ2011-24784), ACIISI (Gobierno de Canarias, ID20100152), and ANPCyT (Argentina, PICT-2010-2554). A. González Orive thank the Spanish MICINN for an FPU grant.

References

[1] J. Mcginnes, P. Corry, P. Proctor, Science 183 (1974) 853–855.
[2] P. Meredith, T. Sarna, Pigment Cell Res. 19 (2006) 572–594.
[3] P. Meredith, B.J. Powell, J. Riesz, R. Vogel, D. Blake, I. Kartini, G. Will, S. Subianto, 2006 Broadband photon-harvesting biomolecules for photovoltaics, in: A.F. Collings, C. Critchley (Eds.), Artificial Photosynthesis: From Basic Biology to Industrial Application, Wiley-VCH Verlag GmbH & Co. KGaA, Weinheim, 2006.
[4] L. Sangaletti, S. Pagliara, P. Vilmercati, C. Castellarin-Cudia, P. Borghetti, P. Galinetto, R. Gebauer, A. Goldoni, J. Phys. Chem. B 111 (2007) 5372.
[5] K.B. Stark, J.M. Gallas, G.W. Zajac, M. Eisner, J.T. Golab, J. Phys. Chem. B 107 (2003) 3061–3067.
[6] B.J. Powell, T. Baruah, N. Bernstein, K. Brake, R.H. McKenzie, P. Meredith, M.R. Pederson, J. Chem. Phys. 120 (2004) 8608–8615.
[7] C.M.R. Clancy, J.B. Nofsinger, R.K. Hanks, J.D. Simon, J. Phys. Chem. B 104 (2000) 7871–7873.
[8] M.M. Jastrzebska, H. Isotalo, J. Paloheimo, H. Stubb, B. Pilawa, J. Biomater. Sci. Polymer Ed. 7 (1996) 781–793.
[9] P. Díaz, Y. Gimeno, P. Carro, S. González, P.L. Schilardi, G. Benítez, R.C. Salvarezza, A. Hernández Creus, Langmuir 21 (2005) 5924–5930.
[10] A. González Orive, Y. Gimeno, A. Hernández Creus, D. Grumelli, C. Vericat, G. Benitez, R.C. Salvarezza, Electrochim. Acta 54 (2009) 1589–1596.
[11] A. Orive, P. Dip, Y. Gimeno, P. Diaz, P. Carro, A. Hernandez Creus, G. Benitez, P.L. Schilardi, L. Andrini, F. Requejo, R.C. Salvarezza, Chem. Eur. J. 13 (2007) 473–482.
[12] E. Kaxiras, A. Tsolakidis, G. Zonios, S. Meng, Phys. Rev. Lett. 97 (2006) 218102.
[13] P. Ghosh, S. Pagliara, P. Vilmercati, C. Castellarin-Cudia, L. Floreano, A. Cossaro, A. Verdini, R. Gerbauer, A. Goldoni, Phys. Rev. B 80 (2009) 174203.
[14] J.P. Perdew, J.A. Chevary, S.H. Vosko, K.A. Jackson, M.R. Pederson, D.J. Singh, C. Fiolhais, Phys. Rev. B 46 (1992) 6671.
[15] H.J. Monkhorst, J.D. Pack, Phys. Rev. B 13 (1976) 5188.
[16] P.E. Blöchl, Phys. Rev. B 50 (1994) 17953.
[17] P.E. Blöchl, P. Margl, K. Schwarz, in: Chemical Applications of Density-Functional Theory, ACS Symposium Series, American Chemical Society, Washington, DC, 1996, pp. 54–69.
[18] G. Kresse, D. Joubert, Phys. Rev. B 59 (1999) 1758.
[19] G. Kresse, J. Furthmüller, Phys. Rev. B 54 (1996) 11169.
[20] X. Wu, M.C. Vargas, S. Nayak, V. Lotrich, G. Scoles, J. Chem. Phys. 115 (2001) 8748.
[21] S. Grimme, J. Comput. Chem. 27 (2006) 1787.
[22] K. Tonigold, A.J. Grob, Chem Phys. 132 (2010) 224701.
[23] A. González Orive, D. Grumelli, C. Vericat, J.M. Ramallo López, L. Giovanetti, G. Benítez, J.C. Azcárate, G. Corthey, M.H. Fonticelli, F. Requejo, A. Hernández Creus, R.C. Salvarezza, Nanoscale 3 (2011) 1708–1716.
[24] S.A. Suárez, M.H. Fonticelli, A.A. Rubert, E. de la Llave, D. Scherlis, R.C. Salvarezza, M.A. Marti, F. Doctorovich, Inorg. Chem. 49 (2010) 6955–6966.
[25] M. Hoon-Khosla, W.R. Fawcett, A. Chen, J. Lipkowski, B. Pettinger, Electrochim. Acta 45 (1999) 611–621.
[26] A. Iannelli, J. Merza, J. Lipkowski, J. Electroanal. Chem. 376 (1994) 49–57.
[27] P. Joshi, V. Shewale, R. Pandey, J. Phys. Chem. C 115 (2011) 22818–22826.
[28] W.K. Chen, M.J. Cao, S.H. Liu, C.H. Lu, Y. Xu, J.Q. Li, Chem. Phys. Lett. 417 (2006) 414–418.
[29] K. Toyoda, Y. Nakano, I. Hamada, K. Kyuho, S. Yanagisawa, Y. Morikawa, Surf. Sci 603 (2003) 2912–2922.
[30] E. Abad, Y.I. Martinez, F. Flores, J.J. Ortega, Phys. Chem. 134 (2011) 044701.
[31] J. Wellendorff, A. Kelkkanen, J.J. Mortensen, B.I. Lundqvist, T. Bligaard, Top. Catal. 53 (2010) 378–383.
[32] H. Yu, L.J. Webb, J.R. Heath, N.S. Lewis, Appl. Phys. Lett. 88 (2006) 252111.
[33] K. Xue, H.P. Ho, J.B. Xu, J. Phys. D 40 (2007) 2886.
[34] J. Tersoff, D.R. Hamann, Phys. Rev. B 31 (1985) 805.
[35] M. Abbas, M. Ali, S.K. Shah, F. D'Amico, P. Postorino, S. Mangialardo, M. Cestelli Guidi, A. Cricenti, R. Gunnella, J. Phys. Chem. B 115 (2011) 11199–11207.
[36] G. Zhang, C.B. Musgrave, J. Phys. Chem. A 111 (2007) 1554.
[37] A.V. Bragas, S.M. Landi, J.A. Coy, O.E.J. Martínez, Appl. Phys. 82 (1997) 4153.
[38] S. Grafström, P. Schuller, J. Kowalski, R.J. Neumann, Appl. Phys. 83 (1998) 3453.